A comparison of structure-activity of Cu-modified over different mesoporous silica supports for catalytic conversion of levulinic acid

Putrakumar Balla (bputrakumar@yahoo.com)
JiangXi University of Science and Technology https://orcid.org/0000-0001-9013-4595
Seelam Prem Kumar
Oulun Yliopisto https://orcid.org/0000-0001-9016-9587
Ginjupalli Srinivasarao
Higher College of Technology Muscat https://orcid.org/0000-0001-8639-1425
Karthikeyan Rajan
JiangXi University of Science and Technology https://orcid.org/0000-0002-9323-4724
Mitta Harishekar
IICT CSIR: Indian Institute of Chemical Technology
Keiski Riitta
Oulun Yliopisto https://orcid.org/0000-0003-2753-7062
Tong Xiang Liang
JiangXi University of Science and Technology

Research Article

Keywords: Copper, Mesoporous silica, Levulinic acid, γ-Valerolactone

Posted Date: March 11th, 2021

DOI: https://doi.org/10.21203/rs.3.rs-248668/v1

Abstract

Catalytic hydrogenation of levulinic acid (LA) to γ-valerolactone (GVL) was investigated over four different types of mesoporous silica (SBA-15, MCM-48, MCM-41, and KIT-6) supported copper (5 wt.%) catalysts. The Cu was incorporated into mesoporous silica supports by a sequential impregnation method. A detailed investigation of the support structure-activity correlation was done and the performance of the catalysts in LA conversion was studied. Detailed characterisation techniques were used to evaluate the physical and catalytic properties of the studied catalysts. The structure type and physicochemical properties of the silica support had a significant effect on the overall performance of the catalysts. Among them, over Cu/SBA-15 catalyst, a complete levulinic acid (LA) conversion with 98% gamma valerolactone (GVL) selectivity was achieved at 265°C under ambient H_2 pressure. The superior performance of Cu/SBA-15 catalyst was due to the high surface acidity, reducibility of Cu oxides species, and highly dispersed Cu particles over SBA-15 structure. The results confirmed that the activity of the catalysts is significantly affected by the textural properties, surface acidity and copper dispersion. Durability of all the catalysts were tested for 50 h time on stream and over the SBA-15 catalyst, only a small drop in the activity was observed.

Statement Of Novelty

In the present work, the novelty and scientific significance lies in introducing the different types mesoporous silica (MS) structures in catalytic hydrogenation of Levulinic acid. We designed and developed a novel and inexpensive catalyst with ultra-fine Cu particles with low and optimal loading over robust mesoporous silica support *i.e.,* SBA-15.

Introduction

Levulinic acid (LA) has been considered as one of the most versatile and renewable molecules produced mainly from lignocellulosic biomass. It has a great potential in biorefinery applications [1–3]. Due to this, considerable efforts are being made and multiple strategies are being proposed for the efficient conversion of LA to value-added compounds and fuels. Among the various transformations of LA, catalytic hydrogenation of LA to γ-valerolactone (GVL)is an important route in the valorisation of biomass platform molecules to specialty chemicals [4, 5]. GVL has been widely used as a sustainable liquid feedstock in the production of transportation fuels and as an additive. Further, GVL acts as a potential monomer in the manufacturing of different kinds of plastics and it can be directly utilized as a green solvent [6]. Moreover, GVL has been used as a hydrogen carrier in the fuel cell applications and also used as a 20% biofuel (produced from GVL) balanced with conventional fuel in the biofuel engine and used in the production of non-enzymatic sugars from biomass.

Catalytic hydrogenation of LA to GVL were studied over a wide variety of noble (Ru, Pt, Pd, Au, and Ir) [7–11], non-noble (Cu, Ni, and Co) [12–14] and bimetallic (RuNi, RuSn,CuFe and CuNi) [15–18] catalysts in both continuous and batch reactor systems under various reaction conditions. Among the catalysts

reported, ruthenium (Ru) based catalytic systems are considered to be the most active and selective in the conversion of LA to GVL in both *i.e.*, homogenous and heterogeneous media [17]. Many reports are focused on non-noble based base metal catalysts due to their cost and abdundance. Developing Cu-based catalysts is more appropriate and industrially viable for the future biorefinery applications. The copper based catalysts are considered to be promising alternatives to the noble metal catalysts, which have shown moderately high performance in the catalytic transformation of LA to GVL. For instance, Upare *et al.* reported over 5 wt.% Cu/SiO_2 catalyst exhibited a complete conversion of LA with 94% GVL selectivity and 6% angelica lactone (AL) at 265°C and 0.1MPa [19]. Lomate *et al.* 2017 studied the effect of Cu modified SiO_2 support with different textural properties of SiO_2 and exhibited varied activities in vapor phase hydrogenation of levulinic acid. They found no correlation between activities and selectivity with support acidity, but strong Cu-support interactions due to partially oxidised Cu species was the main reason for the high activity [20]. Moreover, Rei *et al.*, used a 20 wt.% Cu/SiO_2 catalyst, and achieved 73.4% LA conversion with 75.4% GVL selectivity at 250°C and WHSV of 3.30 h^{-1}[21]. Recently, Sun *et al.* studied three different non-noble metal catalysts *i.e.*, Co, Ni, and Cu based alumina catalysts. Overall, Cu/Al_2O_3 is the most selective catalyst due to the high surface acidity and Cu dispersion [22]. Furthermore, in another study, Cu/Al_2O_3 and Cu/ZrO_2 catalysts were reported in the hydrogenation of LA in a fixed bed reactor at 265°C under ambient pressure and over $Cu/Al_2O_{3,}$ highest catalytic activity in terms of GVL selectivity and LA conversion was gained [23, 24]. In most of the studies, the GVL selectivity was directly correlated to the active metal surface area, surface acidity, and the metal dispersion. Henceforth, designing and developing a highly dispersed, low cost, and abundant Cu-based catalyst in combination with a robust support was the aim of thiswork in LA hydrogenation.

Generally, mesoporous silica supports (SBA-15, MCM-41, MCM-48, and KIT-6) possess high specific surface areas, ordered pore structures, and high thermal stability, which makes them ideal materials for many catalytic reactions. High surface area mesoporous silica (MS) supports can efficiently provide the maximum active sites per mass of catalyst. Moreover, MS supports avoid the diffusion limitations for the reactants and products due to their unique textural properties. However, changing the textural and surface properties of different mesoporous materials can lead to varied catalytic performances[25].

This research work aim is to study the Cu loaded mesoporous silica supported catalysts with different textural properties in a fixed bed reactor atambient pressure. Thus, this work gives an overall correlation between the role of MS textural properties, metal-support interaction, copper dispersion withthe catalytic activity. In the present work, four different types of mesoporous silica supports were synthesized by a hydrothermal method and then copper nanoparticles were deposited by a wet impregnation method. The catalysts characterized by using various analysis techniques and methods such as microscopic, spectroscopic, XRD, UV-DRS, N_2 sorption measurements, SEM, TEM, H_2-TPR, and NH_3-TPD. Active surface area and dispersion of copper were calculated from the N_2O titration method. Catalytic activities were determined in terms of LA conversion, GVL selectivity and catalysts stability.

Experimental

Materials and methods

The parent silica materials (SBA-15, MCM-41, MCM-48, and KIT-6) were synthesized from the study [26]. In the synthesis of SBA-15, 4 g of P123 (Poly(ethylene glycol)-*block*-poly(propylene glycol)-*block*-poly(ethylene glycol) polymer and 9.44 g of KCl were dissolved in 2M HCl solution (~ 90 g). The final solution was stirred for 2h at 35°C until homogeneously mixed. In the next step, 6.44 g of TEOS (Tetraethyl orthosilicate) was added dropwise under continuously stirring for 2h. The complete mixture was then transferred to a sealed Teflon lined container and kept at 100°C for 24 h under static conditions. The resulting precipitate was filtered and washed with deionised water (pH 6.9 ± 0.2) until pH 7.0 ± 0.2 was attained. Further, it was dried for 12 h at 80°C and followed by calcination at 500°C for 6h under air.

For MCM-48, 2.4 g of CTAB (Cetyltrimethylammonium bromide) was mixed with 50 mL of deionized water, 50 mL of C_2H_5OH and 12 mL of NH_3 (32 vol.%). This mixture was stirred until a clear solution was obtained. In the next step, TEOS (3.4 g) wasadded to the mixture and stirred for 2 h. The final product was filtered, extensively washed, dried overnight, and calcined for 6 h at 600°C.

MCM-41 was prepared by using 2.4 g of CTAB dissolved in 120 mLof deionized water and then stirred until a clear solution was visible. After dissolution, 8 mL of NH_3 (32%) was added to the solution, followed by dropwise addition of 10 mL of TEOS and stirring at 35°C for 24 h. The final product was washed with ethanol/H_2O, dried for 12 h at 60°C and calcined for 5h at 500°C.

For synthesis of KIT-6, Pluronic P123 (6 g) was dissolved in 215 mL of deionized water and 11.8 g of HCl (35% v/v) solution under stirring. After dissolution, a 6 g of n-butanol was added dropwise under continuous stirring. Next, a TEOS (12.9 g) was added and stirred at 35°C for 24 h. The final solution was transferred into a sealed Teflon container and subjected to hydrothermal treatment at 100°C for one day. The final solid product was washed, filtered, and dried overnight and next calcined at 500°C for 5h.

The supported copper catalysts with 5 wt.% Cu loading was prepared by a wetness impregnation method. In the typical synthesis procedure, 1.0 g of mesoporous silica support (SBA-15, MCM-41, MCM-48, and KIT-6) was dispersed in 20 mL of aqueous copper nitrate solution and stirred at 60°C. The samples were dried overnight and calcined at 500°C for 5 h. The prepared catalysts were labeled as Cu/SBA-15, Cu/MCM-41, Cu/MCM-48 and Cu/KIT-6.

Catalyst Characterisation

X-ray diffraction patterns were obtained by a D8 X-ray diffractometer (Bruker, Germany) using Cu Kα radiation (-1.5406 A°, 40 kV and 30 mA). Nitrogen sorption measurements were conducted on an Autosorb-1 analyzer (Quanta chrome) at -196^{o}C. Before analysis, the samples were degassed at 250°C for 6h under vacuum. The specific surface area and pore size distribution were measured by using Brunauer-Emmett-Teller (BET) and Barret-Joyner-Halenda (BJH) methods, respectively. The UV-Vis diffused reflectance spectra (UV-DRS) were recorded by a UV-visible spectrometer (GBC scientific-Cintra). Transmission electron microscopy (TEM) images were captured on a Hitachi HT7700 operated at 100 kV

instrument. Scanning electron microscopy (SEM) images were taken on a Philips/Fei Quanta 200F SEM operated at 20 kV instrument.

Hydrogen temperature programmed reduction (H_2-TPR) and temperature programmed desorption of NH_3 (NH_3-TPD) were conducted on micrometric instruments (Auto Chem. 2910). In H_2-TPRexperiment, 0.1 g of sample was pretreated by passing He gas at 200°C for 2 h and then cooled down to ambient temperature. TPR analysis was performed from 25°C to 600°C in a flow of 5% H_2/Ar with a ramping rate 10°C/min. Moreover, in TPD-NH_3 experiment, 0.1 g sample was pretreated by a flow of He gas at 200°C for 2 h followed by saturation with 10% NH_3/He gas at 80°C for 1 h. It was then purged with He gas at 140°C for 2 h. TPD analysis was carried out from 25°C to 600°C at a ramping rate of 10°C/min. Grams/32 software was used to calculate the amount of H_2 consumed and desorbed NH_3 values.

N_2O decomposition experiments were also conducted on micrometric instruments (Auto Chem. 2910). Prior to analysis, the sample was reduced with H_2 gas at 300°C for 3 h followed by He purges for 30 min and then cooled to 80°C. Thereafter, the sample was exposed to 2%N_2O-He for 30 min to oxidize Cu to Cu_2O. Reduction of surface copper oxide was performed by a similar procedure to TPR experiments. Cu surface area, dispersion and crystal size were measured from the total amount of H_2 consumed during the TPR analysis. Copper metal surface area of the catalyst were determined by the following equation.

$$S_{cu} = N_M \cdot N_A \cdot SF / Ns$$

where S_{cu} is the Metal surface area (m^2g^{-1}), $\mathbf{N_M}$ is the Gas adsorbed at monolayer, $\mathbf{N_A}$ is the Avogadro number, **SF** is the Adsorption stoichiometry, and **Ns** is the Number of surface copper atoms per unit area ($1.47 \times 10^{19}\ m^{-2}$).

By assuming copper metal to bespherical crystallites, the particle size can be calculated from following equation: Particle size (A^o) = $6 \cdot 10^4 / (S_{Cu} \cdot \rho_{Cu})$

where ρ_{Cu} is the copper density ($8.92 gcm^{-3}$).

Catalytic activity

The catalytic hydrogenation of LA was performed in afixed-bed glass reactor with 9 mm inner diameter and 32 cm in length over a temperature range from 225 to 300°C at 0.1MPa hydrogen pressure. The catalyst (0.3 g) was mixed with glass beads and loaded at the center of the reactor with glass wool packed from both ends. Beforethe catalytic activity test, the catalyst was pretreated with H_2stream at 350°C for 3 h. After reduction, the reactor temperature was cool down to 265°C and a stream of aqueous solution (10 wt.%) of LA was fed into the reactor along with H_2 at WHSV 0.550 h^{-1}. The reaction products were collected after every hour in an ice trap and later analyzed by GC-MS (HP5973-GC-MSD) by using capillary column (HP-1MS).

Results And Discussion

Low angle XRD patterns of four pure supports (SBA-15, MCM-41, MCM-48, and KIT-6) and their respective Cu impregnated samples have been presented in Figure. 1a and inset in Fig. 1a, respectively.The low-angle diffraction patterns of SBA-15 and Cu/SBA-15 exhibited well-resolved diffraction peaks at around 2q-0.9° corresponds to (1 0 0) reflection of SBA-15 **[27]** and indicating a hexagonal unit cell. The results confirmed that the mesoporous silica structure was well intact after the copper incorporation. However, the impregnation of copper on the silica support resulted in a low intensity peak, which could be ascribed to the scattering phenomenon of metallic copper nanoparticles. The XRD pattern of pure MCM-41 (inset in Fig.1a) shows three wall-separated reflections at 2q-3.7° (a strong intense peak), around 2q-4.5° and 2q-4.7°, denoted as weak intense peaks, corresponding to d_{100}, d_{110} and d_{200} planes, respectively, which was considered as the fingerprints of ordered mesoporous structure **[28]** of MCM-41 materials. After impregnation of copper over the MCM-41 support, the intensity of all XRD peaks decreased considerably due to occupied Cu species in the cylindrical mesopores of the MCM-41 support. The diffraction peaks of MCM-48 and Cu/MCM-48 were found in well agreement with the unique 3D cubic structures of MCM-48 as reported elsewhere **[29]**. Moreover, KIT-6 sample exhibited well-resolved reflections, which were assigned to a well-ordered 3-D cubic Ia3d symmetry of silica structure **[30]**. Further, the 5Cu/KIT-6 sample manifested a cubic structure, which was very similar to its parent sample. All Cu impregnated mesoporous samples exhibited a steady declined in their diffraction peak intensities as compared to their respective parent samples.

Table 1. Textural properties of different mesoporous silica support and the Cu modified catalysts.

Catalyst	Copper loading[a] (wt. %)	BET surface area[b] (m^2/gm)	Pore volume[b] (cc/gm)	Average pore diameter[b] (nm)
SBA-15	-	1062	1.413	5.10
MCM-41	-	759	0.692	3.65
MCM-48	-	1125	0.6075	2.16
KIT-6	-	767	0.8969	4.67
Cu/SBA-15	4.61	764	0.9137	4.78
Cu/MCM-41	4.48	693	0.5971	2.67
Cu/MCM-48	4.51	928	0.5669	2.06
Cu/KIT-6	4.57	524	0.7567	5.77

a-Results obtained from ICP

b-Results obtained from N_2 sorption measurements

The wide-angle XRD patterns of the supported copper samples have been illustrated in Fig.1b. All the XRD patterns shown broad peaks between 2q=15-30°, which were considered as characteristic peaks of amorphous silica. Further, Cu/KIT-6 shown distinguished peaks correspond to CuO (JCPDS 45-0937) at 2q= 32.63°, 35.54°, 38.85°, 48.95°, 53.61°, 58.54°, and 61.73°, respectively. The observed peaks indicated the presence of bulk CuO in KIT-6, however, similar peaks were absent in Cu/SBA-15, Cu/MCM-41and Cu/MCM-48 catalysts. The results suggested that CuO crystallites were highly dispersed over Cu/SBA-15,

Cu/MCM-41 and Cu/MCM-48 catalysts and formed small Cu crystallites (<4nm) over the respective supports.

Moreover, N_2 adsorption-desorption analysis was carried out to determine the specific surface area, cumulative pore volume and average pore size of the prepared catalysts. N_2 sorption isotherms and the respective BJH pore size distribution profiles of pure supports and supported copper catalysts have been presentedin Fig. 2a and Fig. 2b. For all four support catalysts, a sharp enhancement in the adsorbed and desorbed isotherms were displayed in the relative pressure range of 0.6-0.7 for SBA-15, 0.3-0.35 for MCM-41, 0.25-0.35 for MCM-48 and 0.5-0.8 for KIT-6 **[31, 32]**. The isotherms of pure SBA-15 and Cu/SBA-15 exhibited a sharp uptake of N_2 at relative pressures of 0.6-0.8 showing type IV isotherm with H1 hysteresis loop. This indicated the presence of evenly distributed cylindrical narrow pores. The isotherms of pure MCM-41 support and Cu/MCM-41 exhibited typical type IV isotherm with definite elevation in P/P_o range of 0.25-0.35 and 0.3-0.4 due to capillary condensation and spontaneous filling of mesopores, respectively. The isotherm of MCM-48 presented a sharp adsorption atrelative pressure of about 0.25, representing narrow distribution of pores.The specific surface area, pore volume and average pore diameter declined significantly for supported catalysts *i.e.* Cu/SBA-15, Cu/MCM-41 and Cu/MCM-48 catalysts compared to pure support materials (Table1). The incorporation of copper into mesopores resulted in increased density of Cu sites and thus, a considerable decrease in the surface area of supporting material was observed. However, in the case of Cu/KIT-6, the average pore diameter was slightly increased which ascribed the blocking of the small pores **[26]**.

The UV-DRS spectra for all the supported catalysts have been presented in Fig.3. All the catalysts exhibited one common intense absorption band ranging from 200 to 280 nm, which could be originated from the charge transfer transition between ligand O^{2-} and Cu^{2+} in an isolated state **[33]**. Further, a slight shoulder peak was also observed for the Cu/SBA-15, Cu/MCM-48 and Cu/KIT-6 catalysts at around 300 nm, indicating the limited presence of oligomeric cluster-like moieties originating from the charge transfer between Cu^{2+} and O^{2-} in the $(Cu\text{-}O\text{-}Cu)_n$ surface species **[34]**. The charge transfer band of Cu/MCM-48 was found to be more intense and broader compared to other catalysts indicating the formation of mononuclear oxide species in a dispersed state. The broad absorption band with weak intense band was observed between 500-800 nm, and this band was assigned to electron d–d transitions in Cu_{2p} in a octahedral surrounding by the oxygen in CuO particles **[35].**

The TPR profiles and their respective hydrogen consumption values of the supported copper catalysts have been presented in Fig. 4 and Table 2 respectively. From Fig. 4, herein, two similar reduction peaks at ~220°C and ~290°C were observed for Cu/SBA-15 and Cu/MCM-48 catalysts, respectively. The low temperature peak was corresponding to a finely dispersed reduced CuO to Cu, while the high temperature peak was originated from the reduction of bulk CuO species presented in the mesoporous silica supports.

The published reports related to the reducibility of supported copper catalysts have suggested that bulk CuO is hard to reduce as compared to the highly dispersed copper oxides **[36].** In many studies, similar peaks at ~220°C and ~290°C in Cu/MCM-48 corresponds to widely dispersed over support surface and

the bulk CuO species presented inside the structure, respectively. The TPR profiles for the Cu/MCM-41and Cu/KIT-6 consisted a single reduction peak in high temperature region (around 310°C). The profile for Cu/MCM-41 corresponds to the reduction of bulk CuO to metallic copper, while the reduction profile of Cu/KIT-6 suggested the shifting of peak towards higher temperature region due to the existence of copper oxides in the bulk form. Typically, H_2 consumption of Cu/MCM-48 in a low temperature region was found to be relatively high compared to all other catalysts. Thus, indicates that the most of CuO species were highly dispersed over the MCM-48 and SBA-15 supports and that could be easily reduced. The results were found to be in well agreement with the XRD, UVDRS, and textural properties.

Table 2. The maximum peak temperature (T_{max}) and H_2 consumption values of various copper catalysts from TPR analysis and desorbed NH_3 values from TPD results.

Catalyst	T max[1] (^{0}C)	H_2consumption (mmol/gm)	T max[2] (^{0}C)	H_2consumption[a] (mmol/gm)	Total H_2 Consumption[a] (mmol/gm)	Total desorbed[b] NH_3 (mmol/gm)
5Cu/SBA-15	220	96	290	456	552	837
5Cu/MCM-41	-	-	301	482	482	564
5Cu/MCM-48	200	487	279	36	523	671
5Cu/KIT-6	-	-	318	543	543	441

a-Results from H_2-TPR
b-Results obtained from NH_3-TPD

The TPD profiles of supported copper catalysts have been shown in Fig.5 and corresponding data have been summarised in Table 2. All the four catalysts showed one desorption peak below 120°C that is due to the physisorbed NH_3 over the surface of the catalyst. The Cu/SBA-15 and Cu/MCM-48 shown a shoulder peak in between 120-300°C which was attributed to the desorption of ammonia from the weak acid sites **[37].** All the catalysts exhibited broad desorption peaks at higher temperature (i.e., above 300°C) due to the existence of moderate acid sites on the surface. Further, the total surface acidity of the supported mesoporous silica catalysts was found to be in sequence of Cu/SBA-15>Cu/MCM-48> Cu/MCM-41> Cu/KIT-6 (Table 2).

Copper dispersion has been defined as the ratio of the number of copper atoms present over the surface to the total number of copper atoms. The copper dispersion, active metal surface area and crystallitesize of copper supported silica catalysts reported in Table 3. According to the N_2O decomposition results, the H_2 uptake, dispersion, and metal area of the mesoporous silica-supported copper catalysts presented was in the decreasing order: Cu/MCM-48>Cu/SBA-15>Cu/MCM-41>Cu/KIT-6. It was observed that the Cu/MCM-48 catalyst exhibited highest copper surface area and better dispersion compared to other catalysts (Table 3). The reason for this might be the presence of high number dispersed copper sites over MCM-48 surface.

Table 3. Copper dispersion, metal surface area and particle size of different copper supported on mesoporous silica catalysts.

Catalyst	H_2 Uptake (mmol/gm)	Dispersion (%)	Metal area (m^2/gm_{Cu})	Average Particle size (nm)
Cu/SBA-15	132	34	217	3.1
Cu/MCM-41	80	21	132	5.1
Cu/MCM-48	151	39	249	2.7
Cu/KIT-6	61	16	101	6.7

The SEM (Fig. 6) and TEM (Fig. 7) analysis were conducted to determinethe morphologies (shape and size of the pore) of the mesoporous silica-supported copper catalysts. SEM image of SBA-15 displayed multiple rope like domains of relatively uniform in size. MCM-48 comprised of the spherical particles with diameter ranging from 0.3 to 0.5μm while pure KIT-6 support exhibited spherical platelets like morphology. The TEM images of catalysts exhibited a well-defined ordered structure with different sizes. It was noticed that the mesoporous framework of the four samples retained their morphology even after impregnation with copper particles.

Catalytic activity results

Evaluationof the catalytic activity of mesoporous silica-supported copper catalysts was conducted in a continuous fixed-bed reactor at 265°C and 0.1 MPa hydrogen pressure (Table 4). In LA hydrogenation, GVL was found to be the primary and desired product, while angelicalactone (AL) and valeric acid (VA) were produced as the by-products. It was clearly evidentthat the, first LA was dehydrated to AL and then hydrogenated to GVL in the final stage. According to previous reports, over 5 wt.% Cu/SiO_2 shown complete conversion of LA with selectivity to GVL of 94% and AL of 6% at 265°C and 0.1MPa was obtained. Further, in another study, 20 wt.% Cu/SiO_2 catalyst has shown 73.4% LA conversion and 75.4% GVL selectivity at 250°C and WHSV of 3.30 h^{-1}**[21]**. In the present study, we achieved better results with lower Cu loading compared to published data on Cu-based catalysts and overall, 5 wt.% Cu/SBA-15 exhibited complete conversion of LA and 98% selectivity to GVL at 265°C temperature and 0.1MPa hydrogen pressure. Moreover, Cu/MCM-48 possessed high active surface area, Cu dispersion and smaller metallic Cu particle sizes compared to Cu/SBA-15, Cu/MCM-41, and Cu/KIT-6. In addition, Cu/MCM-48 showed higher metal surface area however, a lower catalytic activity was exhibited compared to Cu/SBA-15. This indicated that in case of Cu/MCM-48, a low surface acidity and also narrow pores could not render LA to the pore channels and led to low accessibility to the active sites compared to Cu/SBA-15. The conversion of LA over supported mesoporous silica catalyst was in the sequence of Cu/SBA-15>Cu/MCM-48>Cu/MCM-41>Cu/KIT-6. The order of the LA conversion was observed to be consistent with that of the total surface acidity, thus, exhibiting highest LA conversion for Cu/SBA-15 catalyst. The superior catalytic activity was attributed to the execess availability of the reducible copper species in the

mesoporous channels of the catalysts. Among all catalysts, 5 wt.% Cu/SBA-15 achieved superior performance and displayed complete LA conversion with 98% GVL selectivity.

Table 4. Catalytic performance of differentmesoporous silica supported Cu catalysts.

Catalyst	Conversion (%)	Selectivity (%)			
		AL	GVL	VA	Others
Cu/SBA-15	100	-	98	2	-
Cu/MCM-41	85	16	77	3	4
Cu/MCM-48	92	4	92	2	2
Cu/KIT-6	78	29	69	1	1

Reaction conditions: 10wt.% of aqueous levulinic acid,0.3 g catalyst, WHSV0.550 h^{-1} and H_2 flow 30mL min^{-1} under atmospheric pressure. VA = valeric acid and AL = angelica lactone

Hydrogenation of LA over Cu/SBA-15, Cu/MCM-41, Cu/MCM-48 and Cu/KIT-6 was carried out at different reaction temperatures ranging from 225°C to 300°C (Fig.8). Conversion of LA over the Cu/SBA-15, Cu/MCM-41, Cu/MCM-48 and Cu/KIT-6 catalysts increased from 77% to 100%, 58% to 98%, 64% to 100% and 48 to 88%, respectively, with increasing reaction temperatures from 225°C to 300°C. The conversion attained 100% at temperatures above 265°C, while selectivity to GVL achieved maximum at 265°C. However, the selectivity for AL attained very low at similar temperatures. Cu/SBA-15 and Cu/MCM-48 show higher than 90% GVL selectivity with complete LA conversion, whereas Cu/KIT-6 show low catalytic activity in LA conversion and GVL selectivity. Moreover, the selectivity to GVL decreased and selectivity to VA increased with the temperature (from 265 to 300°C). This trend indicated that higher temperatures (300°C) led to the accelerated reaction and converted GVL into VA. Previous reports concluded similar behavior for the Cu/Al_2O_3 catalyst, which accelerated the dehydration of LA molecules on its surface at high temperatures resulting in the ring opening of GVL and thus, decreased the selectivity towards GVL. Apparently, LA is converted to AL at first followed by its subsequent hydrogenation to GVL. Under the studied reaction conditions, the optimum reaction temperature for converting LA to GVL was 265°C. There are many copper-based catalytic systems reported in the literature with different Cu loadings over the various support materialsand reaction conditions. It is hard to compare all of them with our study due to variation in composition, and operating conditions. However, we collected few relevant data which had similar conditions to this work were summarised in Table 5 and short comparison between the reported Cu-based catalysts with this work was made. Recently, complete LA conversion can be achieved at mild temperature, *i.e.,* below 150° but at high operating pressures **[38].** It was an evident that the trade-off factor between operating temperature and pressure in the LA hydrogenation activity.

Table 5. Comparison of Cu based catalysts reported inthe literature and this work.

Catalyst	Reaction conditions	Hydrogen source & pressure	LA conversion (%)	GVL selectivity (%)	Reference
Cu/SiO_2 -Q6	T = 250°C, m = 0.75 g, LA:FA = 1:2	Formic acid	66	81	[20]
Cu-Ni/Al-Fe	T = 150°C, m = 0.125 g	H_2	95	70	[18]
8 wt.% Cu-12 wt.% Co/Al_2O_3	T = 250°C, m = 0.250 g	H_2	100	99	[39]
20% Cu/Al_2O_3	T = 240°C, m = 0.5 g	H_2	93.7	91.5	[22]
30% Cu–ZrO_2	T = 200°C, m = 0.05 g	H_2, 27 bar		90	[40]
3 wt.% $Cu/Zr_{0.8}$-$Ce_{0.2}$	T = 260°C, m = 0.5 g	Formic acid, 0.5 Mpa	88.5	94.2	[41]
3 wt.% Cu/HTC*	T = 265°C, m = 0.5 g	H_2	87.5	95	[42]
4.7 wt.% Cu/ZrO_2-Al_2O_3	T = 130°C, m = 0.5 g	H_2, 3.0 MPa	100	100	[43]
3 wt.% B 18 wt.%Cu/ZrO_2	T = 150°C, m = 0.2 g	H_2, 3.0 MPa	100	100	[38]
32.3 wt% Cu/5%Al_2O_3-ZrO_2	T = 200°C, m = 0.05 g	H_2, 3.0 MPa	100	100	[44]
5 wt.% Cu/SBA-15	T = 265°C, m = 0.3 g	H_2, 0.1 MPa	100	98	This work

*HTC = hydrotalcite;

In addition, further experiments were carried outto evaluate the stability of mesoporous silica-supported copper catalysts under time on stream of 50 h (Fig.9). Cu/SBA-15 was observed to be more stable with a complete LA conversion with negligible signs of deactivation during 30h time on stream. For the Cu/MCM-41 catalyst, the LA conversion and selectivity was observed to be 85% and 77%, respectively, during 15 h reaction time. However, a drastic decrease in LA conversion (51%) and a slight decrease in GVL selectivity was observed as the TOS reached 50 h. For the Cu/MCM-48 catalyst, the conversion of LA decreased linearly with time for the first 20 h approaching 87% conversion, however, the activity decreased to 53% whenfurther increasing time on stream. The reason behind the activity loss can be ascribed to the possible catalyst deactivation due to the blockage of the catalyst pores. Furthermore, for Cu/KIT-6, the LA conversion and GVL selectivity decreased rapidly during the initial 20 h under stream and attained only 40–50% conversion revealing continuous deactivation during the reaction time. Thus, stability studies of catalysts suggested that Cu/SBA-15 exhibited higher stability compared to Cu/MCM-41, Cu/MCM-48, and Cu/KIT-6 catalysts.

Conclusions

Vapor-phase hydrogenation of LA to GVL was carried out in afixed-bed reactor over different mesoporous silica-supported copper catalysts at ambient hydrogen pressure. From characterisation results, the diffraction patterns and N_2 adsorption-desorption studies revealed that the Cu impregnated catalysts retained their mesoporosity and the support structure was intact. Moreover, XRD results showed the presence of a highly dispersed CuO species over all the catalysts except Cu/KIT-6. The support structure had a profound effect on the activity of the catalyst. The copper modified SBA-15 and MCM-48 had desired properties and presented better performance compared to other catalysts. Overall, the Cu-SBA-15 catalyst exhibited the highest catalytic activity in terms of LA conversion (100%) and GVL selectivity (98%) compared to other prepared catalysts due to its high surface acidity and Cu dispersion.The study further indicated that the copper surface area, acidity and diffusion limitation of reactants into pore channels were the key factors, which influenced the activity of catalysts. The overall activity trend of different mesoporous silica-supported copper catalysts for the LA conversion was found as Cu-SBA-15>Cu-MCM-48>Cu-MCM-41>Cu-KIT-6.

Declarations

Acknowledgments & funding

Dr. Putra Kumaracknowledgesthe Council of Scientific and Industrial Research (CSIR), New Delhi for the award of Senior Research Fellowship (SRF). Dr. Putra Kumar acknowledges funding provided by National Science Foundation of China (Project No.51871114) to carry out the research.

Conflicts of interest/Competing interests

There is no conflict of interest (not applicable).

References

1. Climent MJ, Corma A, Iborra S (2014) Conversion of biomass platform molecules into fuel additives and liquid hydrocarbon fuels. Green Chem 14:516–547. doi: 10.1039/c3gc41492b

2. Wenxiu Cao, Wenhao Luo, Hongguang Ge, Yang Su, Aiqin Wang and TZ (2017) UiO-66 derived Ru/ZrO2@C as a highly stable catalyst for hydrogenation of levulinic acid to γ-valerolactone. Green Chem 19:2201–2211. doi: 10.1039/C7GC00512A

3. Yang Y, Sun C, Brown DE, Zhang L, Yang F (2016) A smart strategy to fabricate Ru nanoparticle inserted porous carbon nano fi bers as highly e ffi cient levulinic acid hydrogenation catalysts †. Green Chem 18:3558–3566. doi: 10.1039/c5gc02802g

4. Touchy AS, Hakim Siddiki SMA, Kon K, Shimizu KI (2014) Heterogeneous Pt catalysts for reductive amination of levulinic acid to pyrrolidones. ACS Catal 4:3045–3050. doi: 10.1021/cs500757k

5. Yan K, Jarvis C, Gu J, Yan Y (2015) Production and catalytic transformation of levulinic acid: A platform for speciality chemicals and fuels. Renew Sustain Energy Rev 51:986–997. doi: 10.1016/j.rser.2015.07.021

6. Yan K, Yang Y, Chai J, Lu Y (2015) Catalytic reactions of gamma-valerolactone: A platform to fuels and value-added chemicals. Appl Catal B Environ 179:292–304. doi: 10.1016/j.apcatb.2015.04.030

7. Dhanalaxmi K, Singuru R, Mondal S, Bai L, Reddy BM, Bhaumik A, Mondal J (2017) Magnetic Nanohybrid Decorated Porous Organic Polymer: Synergistic Catalyst for High Performance Levulinic Acid Hydrogenation. ACS Sustain Chem Eng 5:1033–1045. doi: 10.1021/acssuschemeng.6b02338

8. Gu XM, Zhang B, Liang HJ, Ge H Bin, Yang HM, Qin Y (2017) Pt/HZSM-5 catalyst synthesized by atomic layer deposition for aqueous-phase hydrogenation of levulinic acid to valeric acid. Ranliao Huaxue Xuebao/Journal Fuel Chem Technol 45:714–722. doi: 10.1016/s1872-5813(17)30035-x

9. Mustafin K, Cárdenas-Lizana F, Keane MA (2017) Continuous gas phase catalytic transformation of levulinic acid to γ-valerolactone over supported Au catalysts. J Chem Technol Biotechnol 92:2221–2228. doi: 10.1002/jctb.5258

10. Piskun AS, De Haan JE, Wilbers E, Van De Bovenkamp HH, Tang Z, Heeres HJ (2016) Hydrogenation of Levulinic Acid to γ-Valerolactone in Water Using Millimeter Sized Supported Ru Catalysts in a Packed Bed Reactor. ACS Sustain Chem Eng 4:2939–2950. doi: 10.1021/acssuschemeng.5b00774

11. Yan K, Lafleur T, Jarvis C, Wu G (2014) Clean and selective production of γ-valerolactone from biomass-derived levulinic acid catalyzed by recyclable Pd nanoparticle catalyst. J Clean Prod 72:230–232. doi: 10.1016/j.jclepro.2014.02.056

12. Song S, Yao S, Cao J, Di L, Wu G, Guan N, Li L (2017) Heterostructured Ni/NiO composite as a robust catalyst for the hydrogenation of levulinic acid to γ-valerolactone. Appl Catal B Environ 217:115–124. doi: 10.1016/j.apcatb.2017.05.073

13. Sun P, Gao G, Zhao Z, Xia C, Li F (2014) Stabilization of cobalt catalysts by embedment for efficient production of valeric biofuel. ACS Catal 4:4136–4142. doi: 10.1021/cs501409s

14. Yuan J, Li SS, Yu L, Liu YM, Cao Y, He HY, Fan KN (2013) Copper-based catalysts for the efficient conversion of carbohydrate biomass into γ-valerolactone in the absence of externally added hydrogen. Energy Environ Sci 6:3308–3313. doi: 10.1039/c3ee40857d

15. Wettstein SG, Bond JQ, Alonso DM, Pham HN, Datye AK, Dumesic JA (2012) RuSn bimetallic catalysts for selective hydrogenation of levulinic acid to γ-valerolactone. Appl Catal B Environ 117–118:321–329. doi: 10.1016/j.apcatb.2012.01.033

16. Yan K, Chen A (2014) Selective hydrogenation of furfural and levulinic acid to biofuels on the ecofriendly Cu-Fe catalyst. Fuel 115:101–108. doi: 10.1016/j.fuel.2013.06.042

17. Yang Y, Gao G, Zhang X, Li F (2014) Facile fabrication of composition-tuned Ru-Ni bimetallics in ordered mesoporous carbon for levulinic acid hydrogenation. ACS Catal 4:1419–1425. doi: 10.1021/cs401030u

18. Zhang R, Ma Y, You F, Peng T, He Z, Li K (2017) Exploring to direct the reaction pathway for hydrogenation of levulinic acid into Γ-valerolactone for future Clean-Energy Vehicles over a magnetic Cu-Ni catalyst. Int J Hydrogen Energy 42:25185–25194. doi: 10.1016/j.ijhydene.2017.08.121

19. Upare PP, Lee JM, Hwang YK, Hwang DW, Lee JH, Halligudi SB, Hwang JS, Chang JS (2011) Direct hydrocyclization of biomass-derived levulinic acid to 2-methyltetrahydrofuran over nanocomposite copper/silica catalysts. ChemSusChem 4:1749–1752. doi: 10.1002/cssc.201100380

20. Lomate S, Sultana A, Fujitani T (2017) Effect of SiO2 support properties on the performance of Cu-SiO2 catalysts for the hydrogenation of levulinic acid to gamma valerolactone using formic acid as a hydrogen source. Catal Sci Technol 7:3073–3083. doi: 10.1039/c7cy00902j

21. Yoshida R, Sun D, Yamada Y, Sato S, Hutchings GJ (2017) Vapor-phase hydrogenation of levulinic acid to Γ-valerolactone over Cu-Ni bimetallic catalysts. Catal Commun 97:79–82. doi: 10.1016/j.catcom.2017.04.018

22. Sun D, Ohkubo A, Asami K, Katori T, Yamada Y, Sato S (2017) Vapor-phase hydrogenation of levulinic acid and methyl levulinate to Γ-valerolactone over non-noble metal-based catalysts. Mol Catal 437:105–113. doi: 10.1016/j.mcat.2017.05.009

23. Balla P, Perupogu V, Vanama PK, Komandur VRC (2016) Hydrogenation of biomass-derived levulinic acid to γ-valerolactone over copper catalysts supported on ZrO2. J Chem Technol Biotechnol 91:769–776. doi: 10.1002/jctb.4643

24. Putrakumar B, Nagaraju N, Kumar VP, Chary KVR (2015) Hydrogenation of levulinic acid to γ-valerolactone over copper catalysts supported on γ-Al2O3. Catal Today 250:209–217. doi: 10.1016/j.cattod.2014.07.014

25. Hoffmann F, Cornelius M, Morell J, Fröba M (2006) Silica-based mesoporous organic-inorganic hybrid materials. Angew Chemie - Int Ed 45:3216–3251. doi: 10.1002/anie.200503075

26. Patel A, Shukla P, Rufford T, Wang S, Chen J, Rudolph V, Zhu Z (2011) Catalytic reduction of NO by CO over copper-oxide supported mesoporous silica. Appl Catal A Gen 409–410:55–65. doi: 10.1016/j.apcata.2011.09.024

27. Fulvio PF, Pikus S, Jaroniec M (2010) SBA-15-supported mixed-metal oxides: Partial hydrolytic sol-gel synthesis, adsorption, and structural properties. ACS Appl Mater Interfaces 2:134–142. doi: 10.1021/am900625c

28. Abrokwah RY, Deshmane VG, Kuila D (2016) Comparative performance of M-MCM-41 (M: Cu, Co, Ni, Pd, Zn and Sn) catalysts for steam reforming of methanol. J Mol Catal A Chem 425:10–20. doi: 10.1016/j.molcata.2016.09.019

29. Zhao Q, Shen Y, Wang Q, Tian J, Zhou X, Jiang T (2013) A comparative investigation on the catalytic activity of H-Al-MCM-48 and H-Zr-MCM-48 mesoporous molecular sieve on alkylation of phenol with tert-butyl alcohol. Chem Eng J 230:124–132. doi: 10.1016/j.cej.2013.06.057

30. Prabhu A, Kumaresan L, Palanichamy M, Murugesan V (2009) Synthesis and characterization of aluminium incorporated mesoporous KIT-6: Efficient catalyst for acylation of phenol. Appl Catal A Gen 360:59–65. doi: 10.1016/j.apcata.2009.03.004

31. Frey AS, Hinrichsen O (2012) Comparison of differently synthesized Ni(Al)MCM-48 catalysts in the ethene to propene reaction. Microporous Mesoporous Mater 164:164–171. doi: 10.1016/j.micromeso.2012.07.015

32. Tüysüz H, Lehmann CW, Bongard H, Tesche B, Schmidt R, Schüth F (2008) Direct imaging of surface topology and pore system of ordered mesoporous silica (MCM-41, SBA-15, and KIT-6) and nanocast metal oxides by high resolution scanning electron microscopy. J Am Chem Soc 130:11510–11517. doi: 10.1021/ja803362s

33. Derrien G, Charnay C, Zajac J, Jones DJ, Rozière J (2008) Copper-containing monodisperse mesoporous silica nanospheres by a smart one-step approach. Chem Commun 3118–3120. doi: 10.1039/b804593c

34. Chmielarz L, Kuśtrowski P, Dziembaj R, Cool P, Vansant EF (2006) Catalytic performance of various mesoporous silicas modified with copper or iron oxides introduced by different ways in the selective reduction of NO by ammonia. Appl Catal B Environ 62:369–380. doi: 10.1016/j.apcatb.2005.09.004

35. Chary KVR, Sagar GV, Naresh D, Seela KK, Sridhar B (2005) Characterization and reactivity of copper oxide catalysts supported on TiO2-ZrO2. J Phys Chem B 109:9437–9444. doi: 10.1021/jp0500135

36. Sagar GV, Rao PVR, Srikanth CS, Chary KVR (2006) Dispersion and reactivity of copper catalysts supported on Al 2O3-ZrO2. J Phys Chem B 110:13881–13888. doi: 10.1021/jp0575153

37. Subbaramaiah V, Srivastava VC, Mall ID (2013) Optimization of reaction parameters and kinetic modeling of catalytic wet peroxidation of picoline by Cu/SBA-15. Ind Eng Chem Res 52:9021–9029. doi: 10.1021/ie400124d

38. Li JF, Zhao L, Li J, Li M, Liu CL, Yang RZ, Dong WS (2019) Highly selective synthesis of γ-valerolactone from levulinic acid at mild conditions catalyzed by boron oxide doped Cu/ZrO2 catalysts. Appl Catal A Gen 587:117244. doi: 10.1016/j.apcata.2019.117244

39. Yanase D, Yoshida R, Kanazawa S, Yamada Y, Sato S (2020) Efficient formation of γ-valerolactone in the vapor-phase hydrogenation of levulinic acid over Cu-Co/alumina catalyst. Catal Commun 139:105967. doi: 10.1016/j.catcom.2020.105967

40. Orlowski I, Douthwaite M, Iqbal S, Hayward JS, Davies TE, Bartley JK, Miedziak PJ, Hirayama J, Morgan DJ, Willock DJ, Hutchings GJ (2019) The hydrogenation of levulinic acid to Γ-valerolactone over Cu–ZrO2 catalysts prepared by a pH-gradient methodology. J Energy Chem 36:15–24. doi: 10.1016/j.jechem.2019.01.015

41. Mitta H, Perupogu V, Boddula R, Ginjupalli SR, Inamuddin, Asiri AM (2020) Enhanced production of γ-valerolactone from levulinic acid hydrogenation-cyclization over ZrxCe1-xO2 based Cu catalysts. Int J Hydrogen Energy 45:26445–26457. doi: 10.1016/j.ijhydene.2019.11.149

42. Mitta H, Seelam PK, Chary KVR, Mutyala S, Boddula R, Inamuddin, Asiri AM (2018) Efficient Vapor-Phase Selective Hydrogenolysis of Bio-Levulinic Acid to γ-Valerolactone Using Cu Supported on Hydrotalcite Catalysts. Glob Challenges 2:1800028. doi: 10.1002/gch2.201800028

43. Li J, Li M, Zhang C, Liu CL, Yang RZ, Dong WS (2020) Construction of mesoporous Cu/ZrO2-Al2O3 as a ternary catalyst for efficient synthesis of γ-valerolactone from levulinic acid at low temperature. J Catal 381:163–174. doi: 10.1016/j.jcat.2019.10.031

44. He D, He Q, Jiang P, Zhou G, Hu R, Fu W (2019) Novel Cu/Al2O3-ZrO2 composite for selective hydrogenation of levulinic acid to Γ-valerolactone. Catal Commun 125:82–86. doi: 10.1016/j.catcom.2019.03.029

Figures

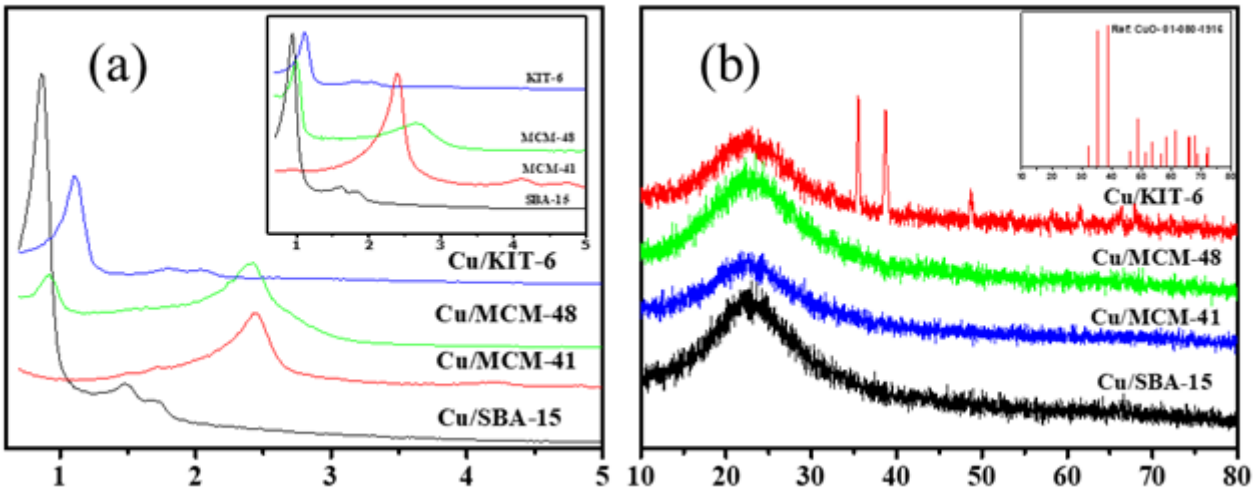

Figure 1

Low angle XRD patternsof various (a) mesoporous silica supported copper catalysts and (inset Figure 1a) parent mesoporous silica and (b)wide angle XRD pattersof various mesoporous silica supported copper catalysts.

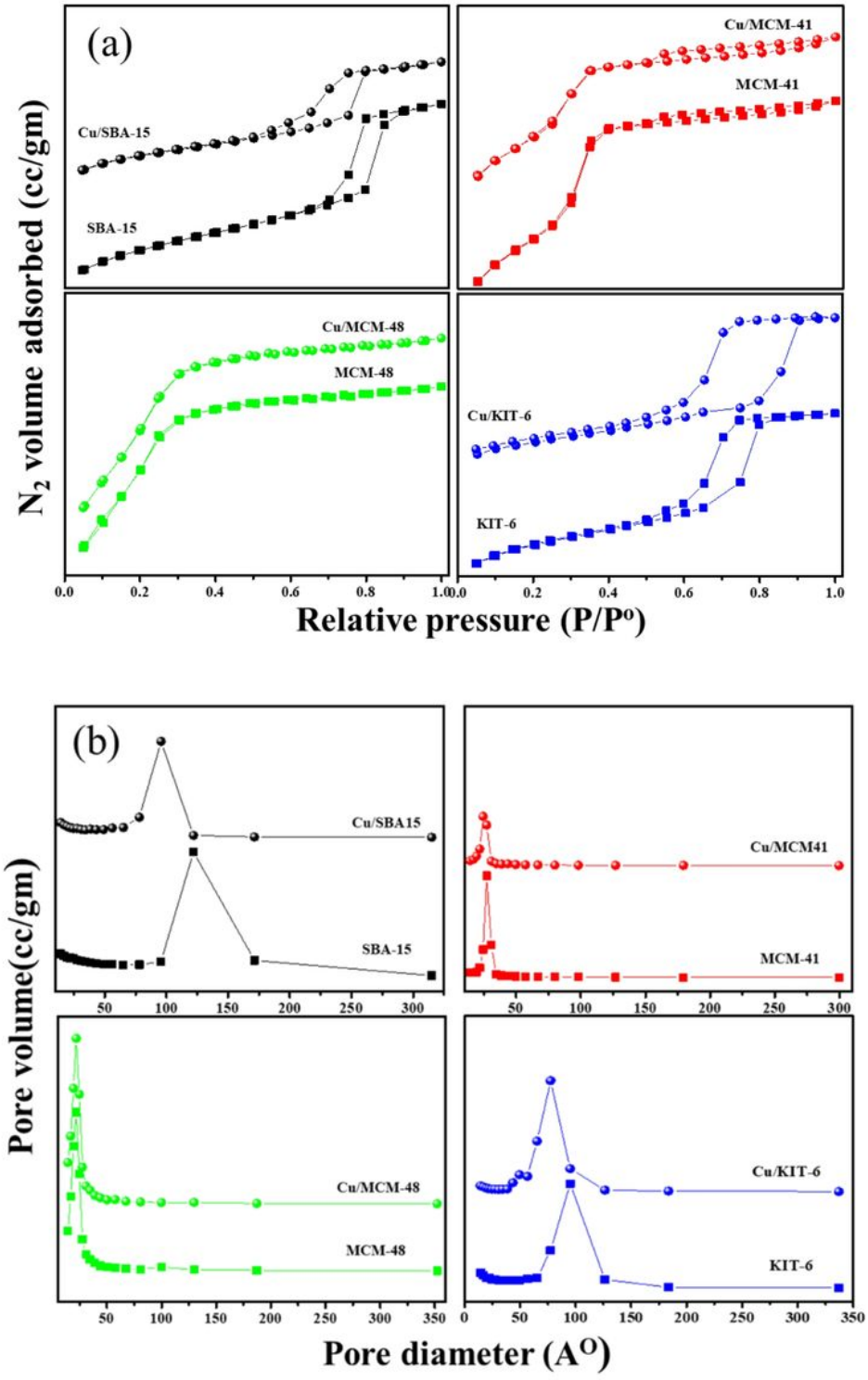

Figure 2

(a) Nitrogen sorption isotherms and the (b) BJH pore size distribution of mesoporous silica supports and the copper supported silica basedcatalysts.

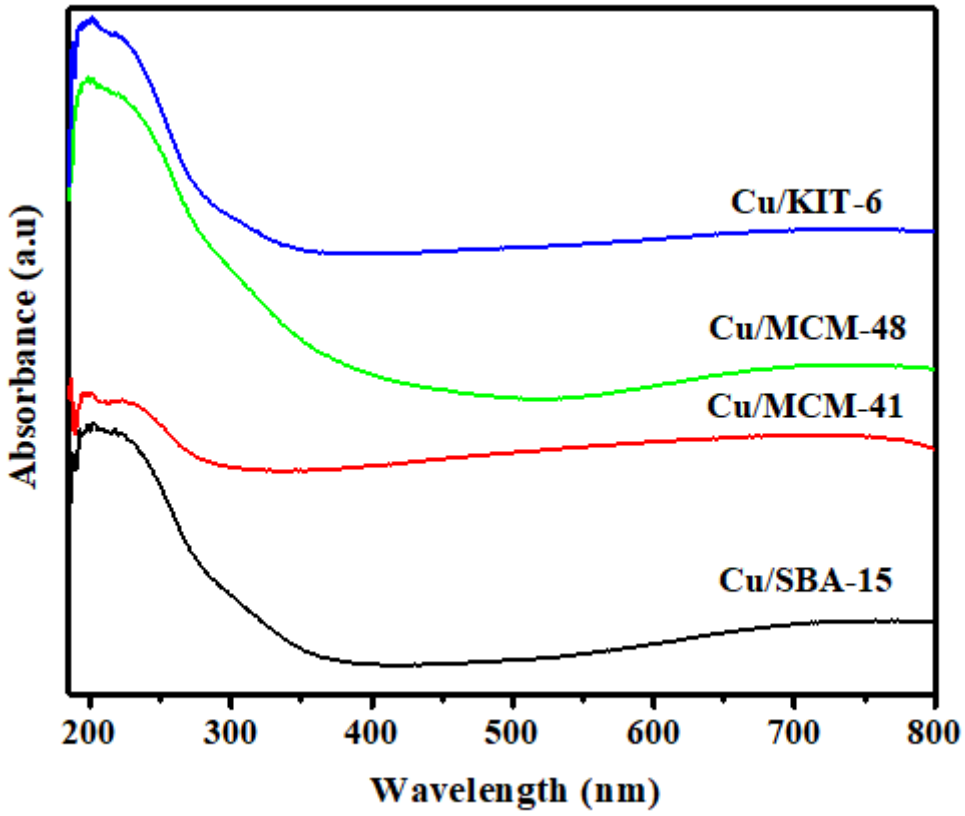

Figure 3

UV-DRS spectra of CuO supported on mesoporous silica catalysts.

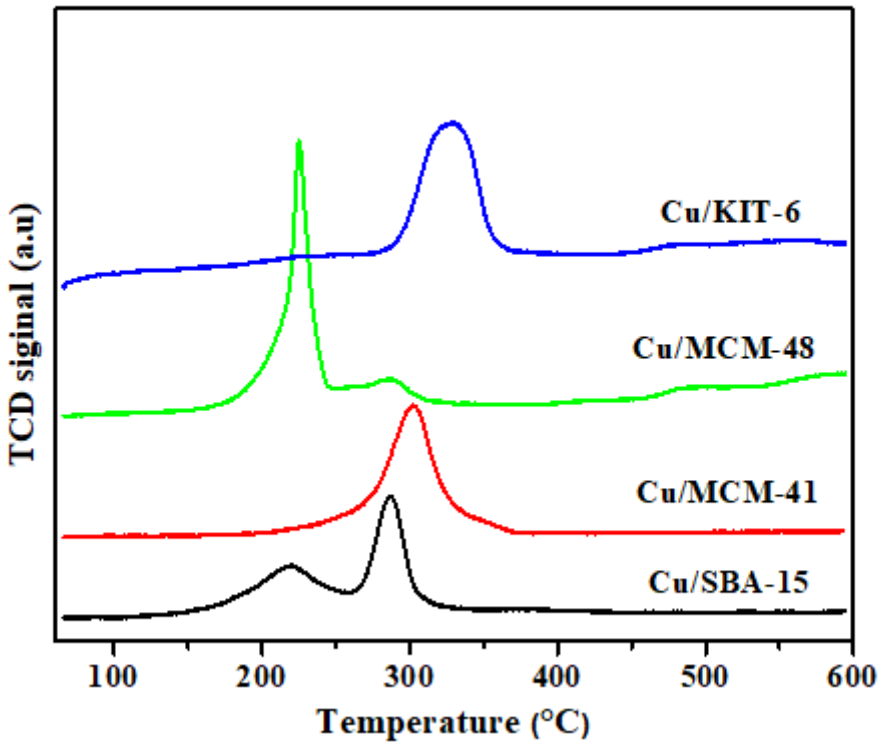

Figure 4

TPR profiles of CuO supported on mesoporous silica catalysts.

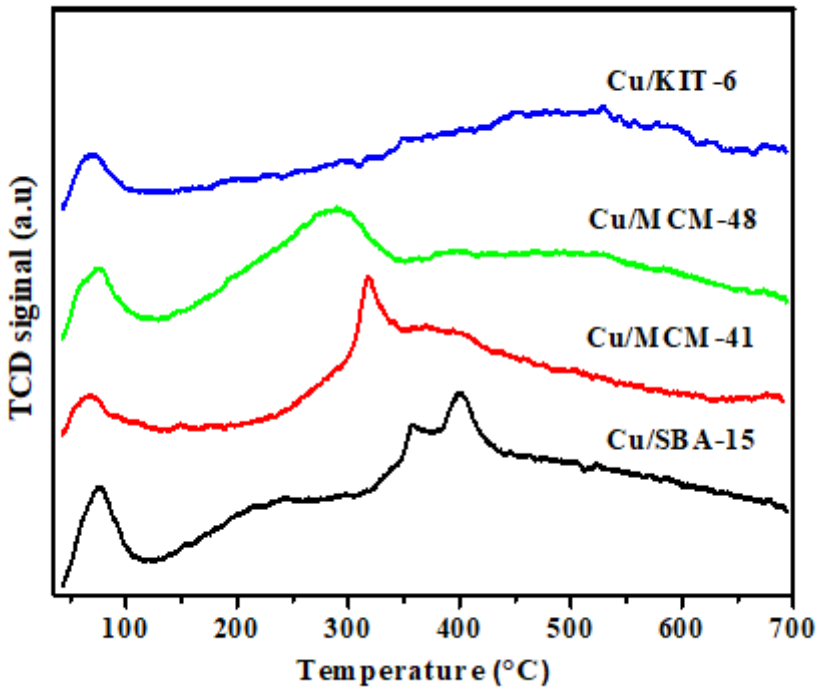

Figure 5

NH3-TPD profiles of CuO supported on mesoporous silicas catalysts.

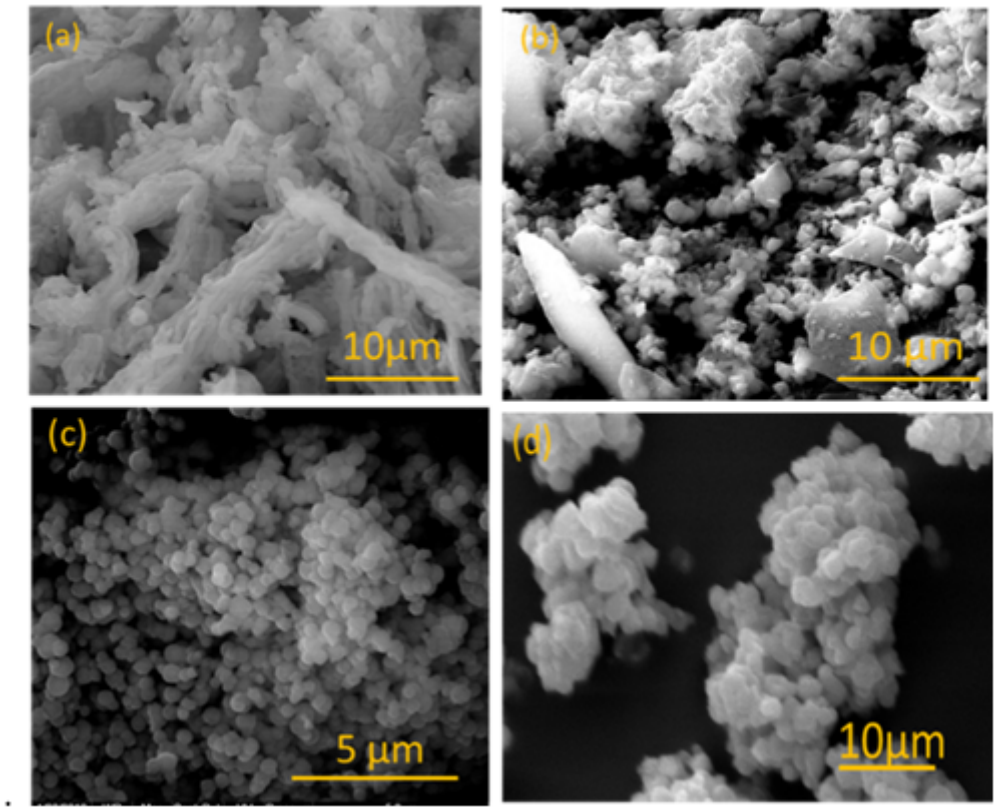

Figure 6

SEM images of (a) Cu/SBA-15 (b) Cu/MCM-41 (c) Cu/MCM-48 (d) Cu/KIT-6 catalysts.

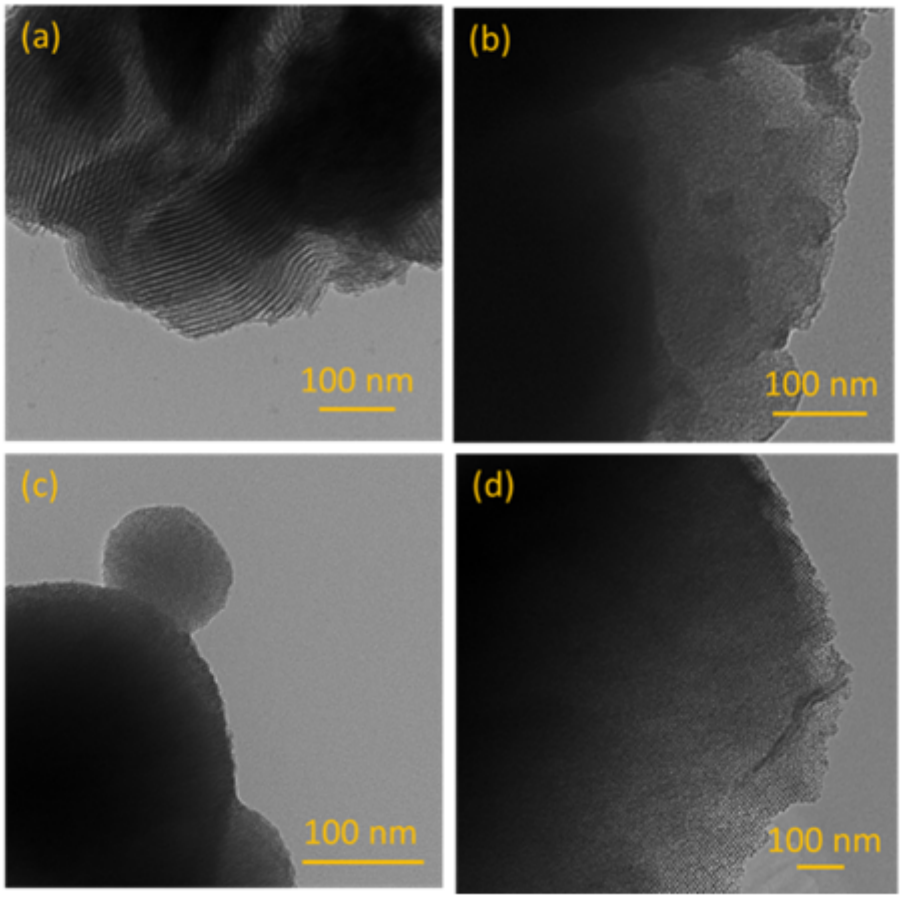

Figure 7

TEM images of (a) Cu/SBA-15 (b) Cu/MCM-41 (c) Cu/MCM-48 (d) Cu/KIT-6 catalysts

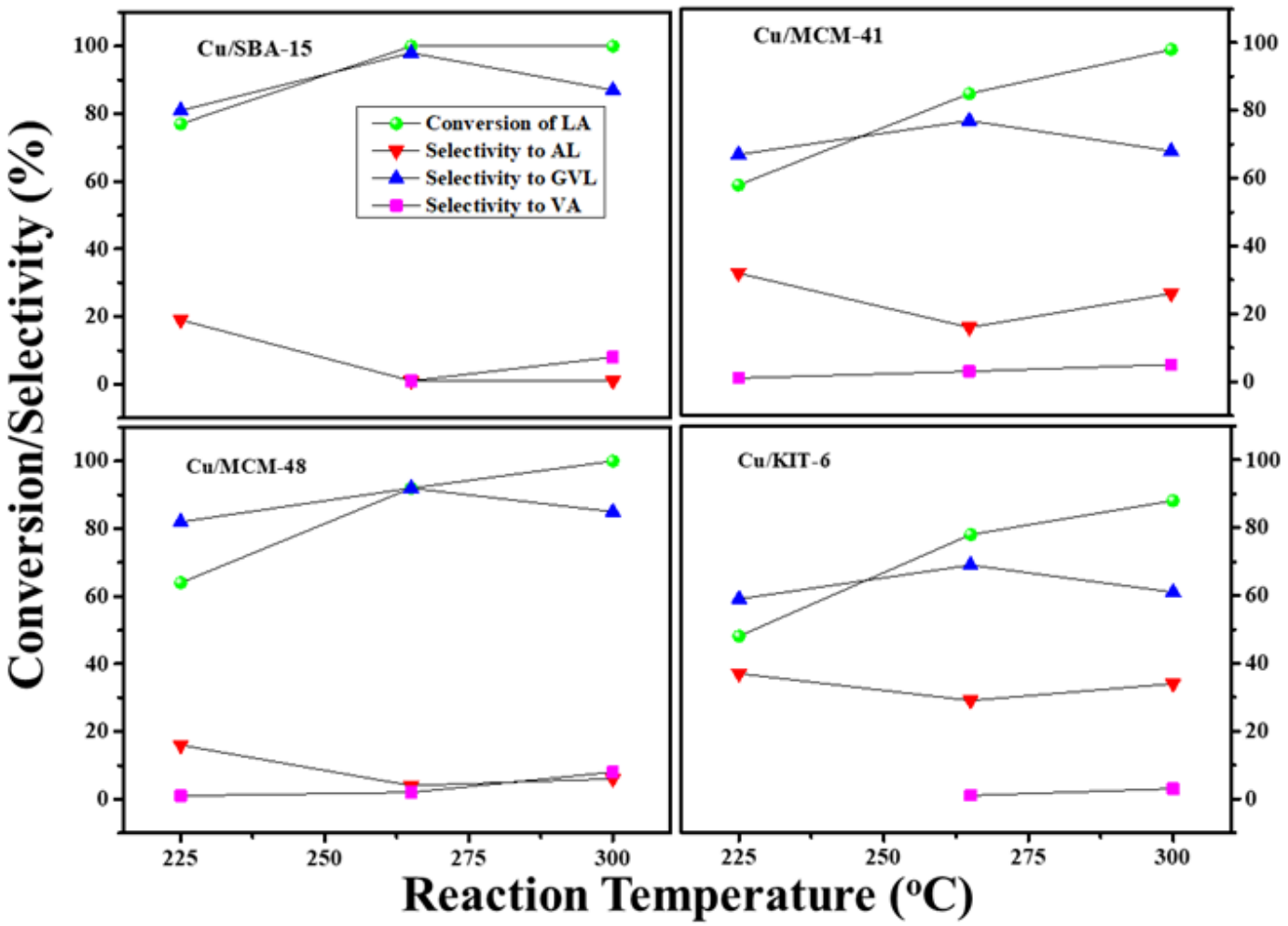

Figure 8

Effect of reaction temperature versus activity in LA conversion and selectivity over the various mesoporous silica supported copper catalysts.

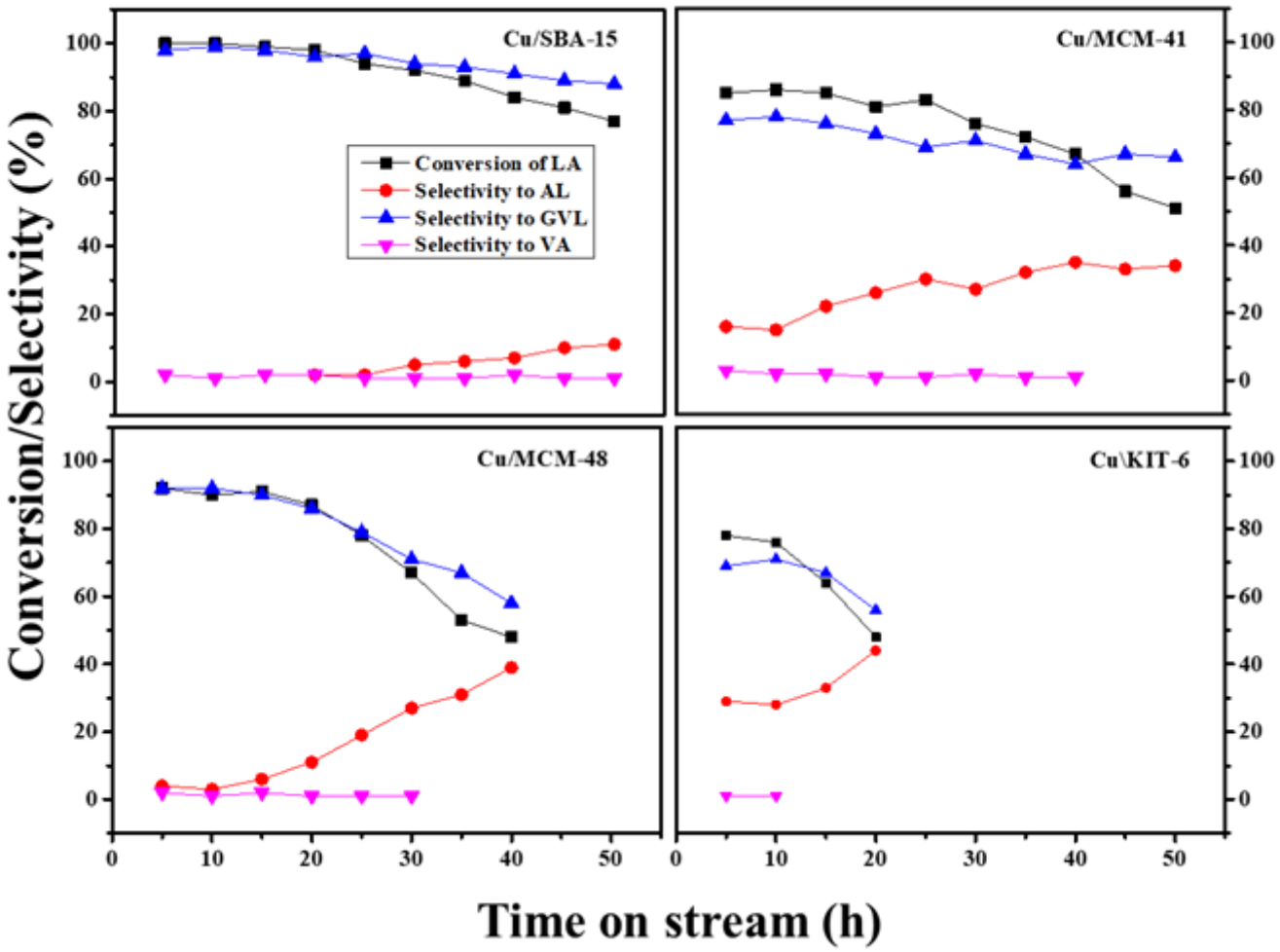

Figure 9

Time on stream studies of various mesoporous silica supported copper catalysts.

Supplementary Files

This is a list of supplementary files associated with this preprint. Click to download.

- Graphicalabstract.tif